ON CONTROL AND PLANNING OF A SPACE STATION ROBOT WALKER

Hiroshi Ueno ** *Yangsheng Xu* *H. Ben Brown, Jr.*
Miyuki Ueno *Takeo Kanade*

The Robotics Institute
Carnegie Mellon University
Pittsburgh, Pennsylvania 15213

ABSTRACT

We are developing a walking robot which can step from one node to the next of a space station trusswork. The 5-DOF robot consists of two light-weight flexible links, configured like an upside-down "V", with a rotary joint at the vertex and a gripper connected by 2-DOF joints at each free end. In walking, the robot attaches the grippers alternately to nodes of the trusswork by screwing into threaded holes in the node. This paper presents the development of control software including the control strategy for the walking motion, low-level control schemes for the robot, and the trajectory planning. We divide one step of the walking motion into four phases: coarse motion, fine motion, insertion, and extraction. In the coarse motion, the robot moves its gripper from one node to the vicinity of another node, during which speed is our main concern. In the fine motion, the robot moves precisely to the top of the hole, and an accurate positioning is desirable in this phase such that the gripper can be inserted into the node. Once the gripper is at the top of hole, it is inserted along the vertical motion to complete one step, and the other gripper is extracted to start the next step. The low-level controllers were designed based on a rigid model added with low-pass filtering. Acceleration feedback was introduced in the control to improve the system bandwidth. A trajectory for our specific walking motion is presented for generating an efficient and stable motion.

1. INTRODUCTION

There are needs for using robots in space applications, such as construction, inspection, transportation, and exploration. In space, robots will be able to autonomously, or by teleoperation, perform many routine tasks that astronauts would otherwise need to do. Robots may also be allowed to work on the tasks that are too dangerous for humans. Using robots in place of humans may eliminate the need for human-support facilities such as air, water, food, etc.

For the purpose of using robots in space, we have undertaken a research project to develop robot technologies in space applications. Currently, we are developing a robot that will walk on the trusswork of the space station, and perform tasks such as transport of tools and materials, inspection of equipment and structures, and assembly of trusswork and equipment. Present efforts are focused on the development of the robot walker and control for primitive movements, and of the gravity compensation system to provide a simulated zero-gravity environment for experiments in the laboratory. We designed and built 1/3 scale laboratory robot and the design considerations were drawn from a hypothetical, full-sized, self contained robot to be used on the space station. Scaling rules were applied so the behavior of the scaled-down robot would be similar to that of the hypothetical one. The detail description of development of the system can be found in another paper in these Proceedings [1].

The robot walker is designed for mobility in a zero-gravity environment, with light weight as primary design goal. The 5-DOF robot consists of two light-weight flexible links, configured like an upside-down "V", with a rotary joint at the vertex and a gripper connected by 2-DOF joints at each free end. In walking, the robot attaches the grippers alternately to nodes of the trusswork by screwing into threaded holes in the node. The kinematic skeleton of the robot structure is shown in Figure 1.

This paper will focus on the development of control software for such a flexible robot walker. In the first section, we will present a control strategy of the walking motion based on the required system performance. Design of low-level controllers is discussed in the second section. The third section details the acceleration feedback method that we employed in walking motion to improve the system performance. In the fourth section, we discusses the trajectory planning problem and presents a special trajectory generator for the walking motion.

2. CONTROL STRATEGY

Control of the robot walker is especially challenging due to the following factors. First, the walker is highly flexible, and structural vibrations are inevitable. Second, joint torques are limited by energy-efficiency and structural considerations, and thus friction in joints becomes a significant factor. Third, tip position sensing is generally not available, yet a high positioning capability of the robot is required so that successful insertion is guaranteed.

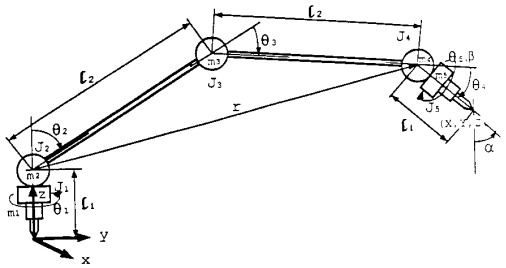

Figure 1 Kinematic skeleton of the robot walker

** Visiting scientist from Space Project Office, Shimizu Corp., Japan.

CH2872-0/90/0000-0220 © $1.00 1990 IEEE

To eliminate the high order vibration of the structure, we used a low-pass filter in joint controllers (see the control diagram in Figure 3). The system bandwidth, however, is decreased by the low-pass filters, and hence the speed of robot motion is greatly limited. We employed acceleration feedback in the coarse motion to eliminate the delay of the digital filter and improve the system performance. The explanation will be given in the section 4.

Joint friction is a significant effect. From experiments, we have found that the torque used for overcoming friction is over 10% of the maximum torque for robot motion. To minimize the nonlinearities due to friction, we used a joint friction compensator which also functions for the compensation of horizontal forces produced by the gravity compensation system as will be discussed in the next section.

To obtain high precision and reasonable speed of locomotion of the flexible structure without tip position sensing, we divided the walking step into four phases: extraction, coarse motion, fine motion, and insertion, illustrated in Figure 2. Our main concern is *speed* in the coarse motion, while it is *precision* in the fine motion. In the coarse motion phase, we used acceleration feedback and low gains for a smooth, stable motion to the area of the target node. Once the gripper is close to the target, the mode switches to the fine motion control using higher gains and integral feedback to minimize the static error. Switching between phases is controlled by the specified position error region. As soon as the gripper is precisely located at the top of hole, the gripper is inserted along the axis of the hole to complete one step, and the other gripper is extracted from the node to start the next step. Experiments have shown that dividing walking motion into different phases is beneficial to achieve positioning precision, motion efficiency, and vibration elimination.

3. LOW-LEVEL CONTROLLER DESIGN

Using the variables defined in Figure 1, we may derive the kinematic relation of the robot walker as follows:

$$\begin{bmatrix} X \\ Y \\ Z \\ \alpha \\ \beta \end{bmatrix} = \begin{bmatrix} -\sin\theta_1(l_2\sin\theta_2+l_2\sin(\theta_2+\theta_3)+l_1\sin(\theta_2+\theta_3+\theta_4)) \\ \cos\theta_1(l_2\sin\theta_2+l_2\sin(\theta_2+\theta_3)+l_1\sin(\theta_2+\theta_3+\theta_4)) \\ l_1+l_2\cos\theta_2+l_2\cos(\theta_2+\theta_3)+l_1\cos(\theta_2+\theta_3+\theta_4)) \\ \pi-(\theta_2+\theta_3+\theta_4) \\ \theta_5 \end{bmatrix} \quad (1)$$

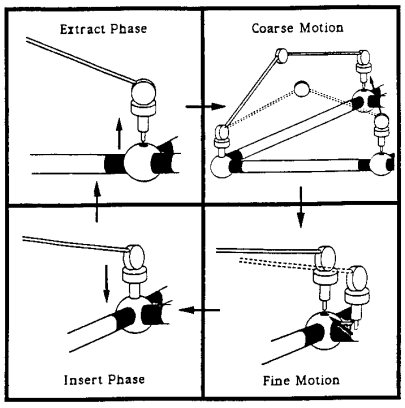

Figure 2 Four phases of the walking motion: extraction, coarse motion, fine motion, and insertion

where θ_i denotes the angle of joint i, and α, β are the angles around the X and Z axes in Cartesian space. For normal walking motion, the angle α is held zero so the gripper keeps vertical direction. In this case, the kinematics can be greatly simplified because $\theta_2+\theta_3+\theta_4$ is equal to π. Hence, the displacements in X, Y, and Z axes are controlled by the joint 1, 2, and 3, while orientations α and β are controlled independently by the joint 4, and 5. Another advantage of this structure is that the inverse kinematics has a closed form solution.

$$r = [(\sqrt{X^2+Y^2}-l_1\sin\alpha)^2+(Z-l_1(1-\cos\alpha))^2]^{1/2} \quad (2)$$

$$\theta_1 = \tan^{-1}(\frac{-X}{Y}) \quad (3)$$

$$\theta_3 = \cos^{-1}(\frac{r^2-2l_2^2}{2l_2^2}) \quad (4)$$

$$\theta_2 = \sin^{-1}(\frac{r}{[\sqrt{X^2+Y^2}-l_1\sin\alpha]^{1/2}})-\frac{\theta_3}{2} \quad (5)$$

$$\theta_4 = \pi-\alpha-\theta_2-\theta_3 \quad (6)$$

$$\theta_5 = \beta \quad (7)$$

From the equations above, it is also clear that the joint 1 or joint 5 is decoupled from joint 2, 3, and 4.

The robot dynamics model can be written in joint space as follows:

$$\tau = \mathbf{I}(\theta)\ddot{\theta}+\mathbf{H}(\theta,\dot{\theta}) \quad (8)$$

where $\mathbf{I}(\theta)$ is 5×5 generalized inertia matrix and $\mathbf{H}(\theta,\dot{\theta})$ is 5-dimensional vector of centrifugal and Coriolis torques. The gravity term in Equation (8) is neglected because of the use of the gravity compensation system. In experiments, using only diagonal terms of inertia matrix, i.e., neglecting both off-diagonal terms of inertia matrix and nonlinear centrifugal and Coriolis torques, yielded a fairly reasonable result. This may be explained in the papers [2] and [3] by the fact that reducing the inertia coupling term can induce a reduction of the nonlinear term. In other words, ignoring both the coupling inertia term and the nonlinear term is better than ignoring either one of them. The diagonal terms of the inertia matrix are

$$I_{11} = n_1^2I_m+m_3(l_2\sin\theta_2)^2+m_4(l_2\sin\theta_2+l_2\sin(\theta_2+\theta_3))^2 +m_5(l_2\sin\theta_2+l_3\sin(\theta_2+\theta_3)+l_1\sin(\theta_2+\theta_3+\theta_4))^2 \quad (9)$$

$$I_{22} = n_2^2I_m+2m_4l_2^2(1+\cos\theta_3)+m_5[2l_2^2(1+\cos\theta_3)+l_1^2 +2l_1l_2\sqrt{2(1+\cos\theta_3)}\cos(\theta_2+\theta_3+\theta_4)] \quad (10)$$

$$I_{33} = n_3^2I_m+m_5(l_1^2+l_2^2)+2m_5l_1l_2\cos\theta_4 \quad (11)$$

$$I_{44} = n_4^2I_m+m_5l_1^2 \quad (12)$$

$$I_{55} = n_5^2I_m \quad (13)$$

where n_i is the gear ratio at joint i using a harmonic drive, and I_m is motor inertia. The off-diagonal terms and nonlinear terms are omitted for simplicity.

The joint controller was designed based on a rigid arm model as shown in Figure 3. A low-pass filter was used for the first three joints to eliminate high-mode vibration of the flexible links, but was not used for the last two joints which have no significant flexibility. The structural vibration modes associated with joint 2 and 3 are around 80 (rad/sec), while that for the joint 1 is around 18 (rad/sec). Thus the corner frequency of the filter for the joint 1 is lower than that for the joint 2, and 3, and the order of the digital filter is also higher than that for the joint 2 and 3. The lower frequency filter presents a significant delay which

results in reducing the usable bandwidth. Therefore, our main concern is how to improve the response of the joint 1 such that the first three joints possess similar responses, making the response of the three translational displacement nearly identical.

The solution for this problem is to introduce acceleration feedback at the first joint controller to improve its bandwidth. The rationale will be explained at the next section. At the same time, a relatively low gain is selected to obtain a reasonable ratio of the desired closed-loop frequency and filter corner frequency, such that the low-mode vibration is prevented and stable walking is maintained. The controller is designed in joint space with a feed-forward loop. A friction compensator is designed to yield an additional torque to overcome the significant joint friction, and a positive or negative value of the torque is generated based on the position error sign.

4. ACCELERATION FEEDBACK

As discussed above, the acceleration feedback loop is introduced in the first joint controller during the coarse motion phase. The block diagram of the control scheme is shown in Figure 4. The robot is represented as a second-order system working in a relatively low frequency region. The desired closed-loop frequency is represented as ω_c and desired damping ratio is ζ_c. A n-order low-pass digital filter with a corner frequency ω_f is employed for eliminating a high-mode vibration of the structure. We use the acceleration feedback K_a to eliminate the response delay and thus improve the system bandwidth.

From the control diagram in Figure 4, using a second-order filter for simplicity, we may obtain the system transfer function:

$$\frac{\theta}{\theta_r} = \frac{(s^2+2\zeta_c\omega_c s+\omega_c^2)\omega_f^2}{s^4+2\omega_f s^3+\omega_f^2(1+K_a)s^2+2\zeta_c\omega_c\omega_f^2 s+\omega_c^2\omega_f^2} \qquad (14)$$

From the transfer function, the stability condition can be derived using the Routh-Hurwitz criterion as follows:

$$(1+K_a)\frac{\zeta_c}{1+\zeta_c^2} > \frac{\omega_c}{\omega_f} \qquad (15)$$

If a unit damping ratio is desired, the condition becomes

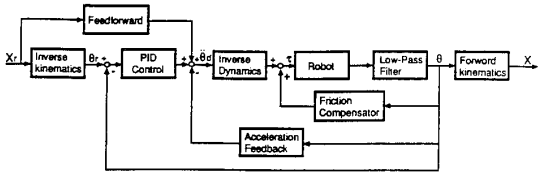

Figure 3 Block diagram of robot controller

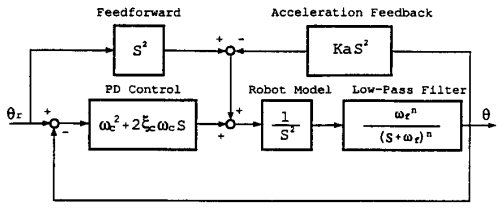

Figure 4 Block diagram of acceleration feedback control

$$(1+K_a) > 2\frac{\omega_c}{\omega_f} \qquad (16)$$

We may see from Equation (16) that introducing the acceleration feedback improves the stability condition. This is true, especially when the closed-loop frequency is close to the corner frequency of the filter. Simulation with the ratio of the frequencies ($\omega_f/\omega_c = 5$) in Figure 5 with various acceleration feedback gains K_a has shown that, using the acceleration feedback, the bandwidth is greatly increased. Figure 6 shows the experimental results with and without acceleration feedback for the joint 1. The tip vibration near the target is effectively eliminated.

5. TRAJECTORY PLANNING

The goal of trajectory planning for the robot walker is to provide a stable and reasonably fast motion. Currently, the software can generate nine types of trajectories for different motion phases. For example, a simple parabolic trajectory can be produced by specifying the settling-time or desired acceleration, either in joint space or Cartesian space, and has been shown good performance in the coarse-motion control. A constant velocity linear trajectory, as another example, was a proper choice for the fine motion control. Application of such trajectories is straight forward. In this section, we will focus on a simple planar motion trajectory designed particularly for our robot walking in the coarse motion.

The tip of the robot during the coarse motion is basically on the x-y plane. The top and side views of the robot mechanism can be shown in Figure 7, using the polar (r–Θ) coordinates. Our plan is to apply discrete values of torques at joints which is constant in amplitude and either positive or negative, i.e., $\pm\tau_{ref}$, dependent on the switching time, in such a way that a maximum allowable acceleration can be used in both radial and circular directions. For simplicity, we assume the mass is concentrated at the tip, since the mass at joint 2 is relatively much less than that at the tip contributed by the gripper and two joints. We only consider "node-to-node" motion, i.e., the initial and end points of the Θ are at 0°, 90°, or 180°. We will ignore centrifugal effects, which allows us to find a radial (r) trajectory independent of the circular (Θ) trajectory. The Coriolis term is included. From Figure 7, it is easy to obtain force and motion relations as follows.

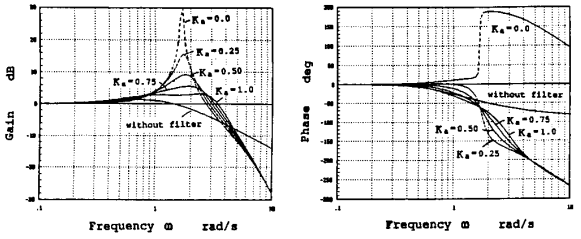

Figure 5 Bode diagram of acceleration feedback control

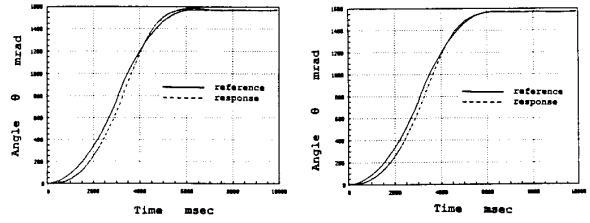

(a) without acceleration feedback (b) with acceleration feedback

Figure 6 Experimental results with and without acceleration feedback

$$F_r = \frac{S_3\tau_3}{l\cos\theta_2} \tag{17}$$

$$F_\Theta = \frac{S_1\tau_1}{2l\sin\theta_2} \tag{18}$$

while

$$F_r = m(\ddot{r} - r\dot{\Theta}^2) \tag{19}$$

$$F_\Theta = m(r\ddot{\Theta}) + 2\dot{r}\dot{\Theta}) \tag{20}$$

where S_1, $S_3 = \pm 1$, and τ_i is the torque of the joint i. Neglecting the centrifugal term ($r\dot{\Theta}^2$), we have

$$\ddot{r} = \frac{S_3\tau_3}{ml\cos\theta_2} \tag{21}$$

$$\ddot{\Theta} = \frac{S_1\tau_1}{2mr\sin\theta_2} - \frac{2\dot{r}\dot{\Theta}}{r} \tag{22}$$

By defining a dimensionless time variable

$$\phi = \sqrt{\frac{\tau_3}{ml^2}}\ t \tag{23}$$

we make the results more general. Now

$$\frac{dF}{dt} = \frac{dF}{d\phi}\frac{d\phi}{dt} = \frac{dF}{d\phi}\sqrt{\frac{\tau_3}{ml^2}} \tag{24}$$

$$\frac{d^2F}{dt^2} = \frac{d^2F}{d\phi^2}\left(\frac{\tau_3}{ml^2}\right) \tag{25}$$

Thus, Equations (21) and (22) can be simplified.

$$\rho'' = \frac{d^2\rho}{d\phi^2} = \frac{S_3}{2\cos\theta_2} \tag{26}$$

$$\Theta'' = \frac{d^2\Theta}{d\phi^2} = \frac{1}{\rho}\left(\frac{S_1\tau}{4\sin\theta_2} - 2\rho'\Theta'\right) \tag{27}$$

where $\rho = r/2l$ and $\tau = \tau_1/\tau_3$.

We use the maximum allowable torque τ_1 (driving Θ) which is positive for the first half of cycle and negative for the second half as shown in Figure 8. The switch point (t_1) and amplitude of τ_3 (driving r) will be selected to give $\dot{r} = 0$ and $r \geq r_{min}$ at the midpoint (t_2). Given the initial parameters $\rho(0)$ and $\theta_2(0)$, a numerical integration algorithm over small increments of dimensionless time ($\Delta\phi$) is used for Equation (26), and $\rho(\phi)$ can be generated for $\phi < \phi_2$. The second half ($\phi > \phi_2$) will be symmetrical about ϕ_2. Once we have computed a trajectory of $\rho(\phi)$, we need to find the value of $\tau = \tau_1/\tau_3$ which gives the desired sweep angle ($\Theta(\phi_2) = 45°, 90°$). We do this by trial and error, i.e., selecting τ, and integrating to get $\Theta(\phi_2)$, adjust τ and try again until $\Theta(\phi_2)$ goes to the desired angle. We may also program this process to generate τ automatically using numerical difference. When the increment is sufficiently small, integration will be convergent.

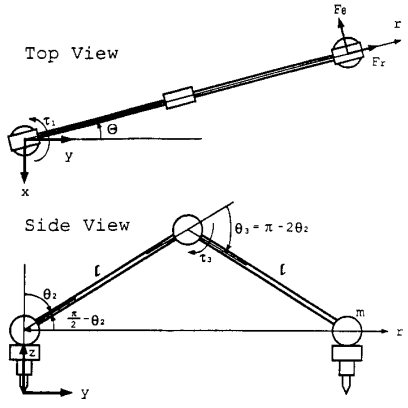

Figure 7 Robot configuration in Polar Coordinates

In the same manner, we can get circular trajectory. A family of trajectories in the x-y plane is shown in Figure 9 for 180 degree motion.

6. CONCLUSIONS

We have developed the 5-DOF robot walker on trusswork of the proposed space station. We presented a control strategy for this flexible, light-weight structure. Experimental results have shown its feasibility in achieving a reasonable speed and stability of motion. Based on the kinematic and dynamic models of the robot, we proposed a joint controller with conventional PID scheme, acceleration feedback, low-pass filter, and friction compensator. Acceleration feedback is successfully employed in the controller such that the system performance is improved. An algorithm to generate a simple trajectory for a planar walking motion has been presented.

7. REFERENCES

[1] H.B. Brown, Jr., M. Friedman, and T. Kanade, "Development of a 5-DOF walking robot for space station application", *Proceedings of IEEE International System Engineering Conference*, 1990, Pittsburgh.

[2] H. Asada, "A geometrical representation of manipulator dynamics and its application to arm design", *ASME Trans, J. Dyn. Syst. Meas. and Control*, Vol. 105, pp. 131-135, 1983.

[3] V.D. Tourassis and C.P. Neuman, "The inertial characteristics of dynamic robot models", *Mechanism and Machine Theory*, Vol. 20, No.1, pp.41-52, 1985.

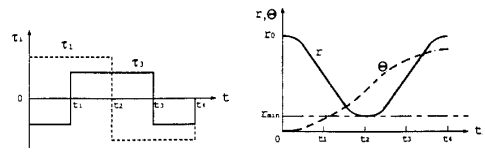

Figure 8 Desired torques and trajectories for radial (joint 1) and circular (joint 3) motion

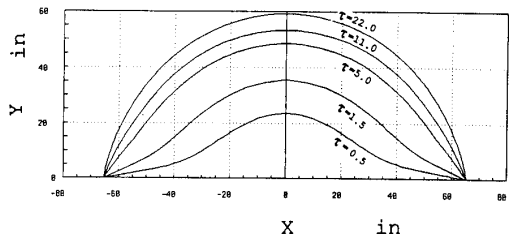

Figure 9 180 degree motion trajectories with different parameters.